

Low-Cost Hydrothermally Synthesized Multifunctional Rare Earth Metal Yttrium Cerium Oxide [†]

Shivangi Srivastava *  and Narendra Kumar Pandey

Department of Physics, University of Lucknow, Lucknow 226007, India; profnarendrapandey137@gmail.com

* Correspondence: shivangsrivastav007@gmail.com

† Presented at the 4th International Online Conference on Nanomaterials, 5–19 May 2023; Available online: <https://iocn2023.sciforum.net>.

Abstract: In this study, YCeO nanocomposites were efficaciously synthesized by the hydrothermal method in the company of sodium hydroxide as a reducing agent as well as cerium nitrate and yttrium nitrate as precursors. Synthesis temperature and pressure, during hydrothermal reactions, show a critical role in governing the shape, size, oxygen vacancy attentiveness, and low-temperature reducibility in CeO₂-based nanocomposites. The lattice constants of the yttrium ceria nanocomposite also are contingent upon the attentiveness of hydroxide ions which primes better morphology at low temperature and pressure. The X-Ray Diffraction (XRD) pattern of YCeO shows the cubic structure of space group Fm3m, having a density of 6.74 gm cm⁻³, volume of 157.81 × 10⁶ pm³, crystallite size of 18.66 nm, and lattice strain of 0.0041, and many more structural parameters were calculated. Field Emission-Scanning Electron Microscopy (FE-SEM) and Atomic Force Microscopy (AFM) studies show the granular structure and surface roughness. Surface porosity and specific surface area were observed by Brunauer–Emmett–Teller (BET), average nanoparticle size was analyzed by the analyzer, and optical properties were observed by Fourier Transform Infrared Spectroscopy and UV-Visible spectroscopy in which the presence of functional and carboxyl group were analysed by FTIR and absorption wavelength 256.58 nm and band gap 3.27 eV were analysed by UV-Visible spectroscopy, lastly thermal stability of this nanoparticle was analyzed by Thermo-Gravimetric Analysis (TGA).

Keywords: cerium oxide; yttrium oxide; nanocomposite; hydrothermal; morphology



Citation: Srivastava, S.; Pandey, N.K. Low-Cost Hydrothermally Synthesized Multifunctional Rare Earth Metal Yttrium Cerium Oxide. *Mater. Proc.* **2023**, *14*, 26. <https://doi.org/10.3390/IOC2023-14542>

Academic Editor: José Luis Arias Mediano

Published: 5 May 2023



Copyright: © 2023 by the authors. Licensee MDPI, Basel, Switzerland. This article is an open access article distributed under the terms and conditions of the Creative Commons Attribution (CC BY) license (<https://creativecommons.org/licenses/by/4.0/>).

1. Introduction

Rare earth metal oxides are very rousing materials due to their exclusive optical, electronic, and magnetic properties [1]. All these chattels lead to many real-world applications such as optics communications, optical displays, efficient catalysis, UV shielding, medical diagnosis, and industries [2]. Therefore, it primes extensive high-tech applications to occur because the quantum efficiency is too low [3]. In general, all of these applications necessitate nanoparticles to have explicit possessions. Cerium oxide nanoparticles have advanced tremendously in the fields of biomedical sciences and industry, among others; not only have all of these applications been verified to be obligatory for humans, but they are also playing a noteworthy role in the worldwide economic growth of many businesses. The studies conducted in this expanse have provided decisive evidence of the signs of progress and establishment. On the other hand, yttrium oxide nanoparticles have many uses in the dominion of materials research, including coloring television picture tubes, flat panels, plasma displays, strong microwave filters, and many more. A critical starting point for the inorganic amalgamation of chemicals is yttrium oxide, which also has the capability to emanate red light, a feature employed in fluorescent lighting. In addition, it has a great application in X-ray and X-ray sensors that exploit ultrafast sensors and many more additional applications.

However, there are presently fewer reports on the investigation of novel CeO₂/Y₂O₃ composite materials with cubic structure and mesopores, which are intriguing scenarios for

a variety of applications due to their massive surface area, stability, and low noxiousness. Several procedures have been working to create nanocomposites with the anticipated properties, together with co-precipitation [4], sol-gel [5], solvothermal [6], sonochemical [7], electrochemical approach [8], sputtering [9,10], arc-discharge [11], and solvothermal [7]. In light of this, we designated the synthesis and properties of cerium/yttrium oxide nanoparticles made using the hydrothermal method, a straightforward technique for creating nanocrystals from aqueous solutions at low temperatures and high vapor pressures in an autoclave lined with Teflon. After that XRD, FE-SEM, AFM, nanoparticle size analyzer, FTIR, UV-visible, BET, and TGA characterizations were performed for a complete understanding the nature and behaviour of the as prepared YCeO.

2. Materials and Methods

In this present work, high-purity chemical reagents were of srl grade after being used without further purification. We use hydrothermal synthesis for the preparation of conflation of nanoparticles, a sufficient amount of 0.1 M cerium (III) nitrate hexahydrate ($\text{Ce}(\text{NO}_3)_3 \cdot 6\text{H}_2\text{O}$) and 0.1 M yttrium (III) nitrate hexahydrate ($\text{Y}(\text{NO}_3)_3 \cdot 6\text{H}_2\text{O}$) were dissolved in distilled water for 6 h to create the homogeneous solution. At the same time, 0.5 M of NaOH was dissolved in distilled water until it completely dissolved. Then NaOH was added dropwise slowly to the previous solution at room temperature until the pH became 10–11 with continuous stirring to attain a completely homogeneous solution. After that, the complete mixture was transferred into a 100 mL Teflon-lined autoclave and placed in an oven at 160 °C for 8 h. Then the autoclave was taken outside and allowed to cool at room temperature, a little pale-yellow precipitate was formed, which was kept in the oven at 100 °C for drying. Thus, the obtained powder was annealed at 550 °C then allowed to cool at room temperature, and powdered nanocomposite YCeO was formed, mixed with cerium/yttrium nanocomposites which are given in the following chemical Equations (1) and (2).



3. Result and Discussion

3.1. XRD Analysis

Powder X-ray diffraction, a non-destructive analytical technique for identifying the multiple crystalline phases of binary metal oxide nanocomposite, was used to examine the crystalline phase of the samples as prepared. Using a powder diffractometer and Cu-K radiations with a 2-theta range of 10°–80°, it was captured. The phases of cerium oxide or yttrium oxide were found among all the recorded peaks from the XRD pattern, and it is evident that all the diffraction peaks are precisely coincident with the cubic phase of bi-nary metal oxide [12,13]. Additionally, it demonstrates the produced nanoparticles' excellent crystallinity and single phase of cubic fluorite crystal structure in the (Fm3m) space group. The X-ray diffraction was performed to obtain the crystal and phase structure of the yttrium cerium oxide, that X-ray pattern was shown in Figure 1, different 2 θ peaks were observed at 28.587, 33.128, 47.553, 56.427, 59.179, 69.524, 76.827, and 79.207 attributed to the (111), (200), (220), (311), (222), (400), (331), and (420) miller indices corresponding to the cubic structure of YCeO. The crystal structure shown in Figure 2 was obtained from XRD data and was designed by Vista software [14]. Here I can show the crystal structure of yttrium oxide [15], cerium oxide [16], and then the nanocomposite of yttrium cerium oxide [17] crystal structure by combing both structures. After that, I will show a single layer of yttrium cerium oxide for a better understanding of the atomic layer structural sites. Lastly, the multilayer cubical/slab structure of yttrium cerium oxide was also shown here to see and understand the surface structure. Then, a slab structure multi-layered structure was finally shown for a better understanding of the complete crystal structure, which was

built after the composition of both nanomaterials. Different parameters were obtained such as volume density, space group, lattice/grain size, and many more calculated by refinement and different formulas as tabulated in Table 1.

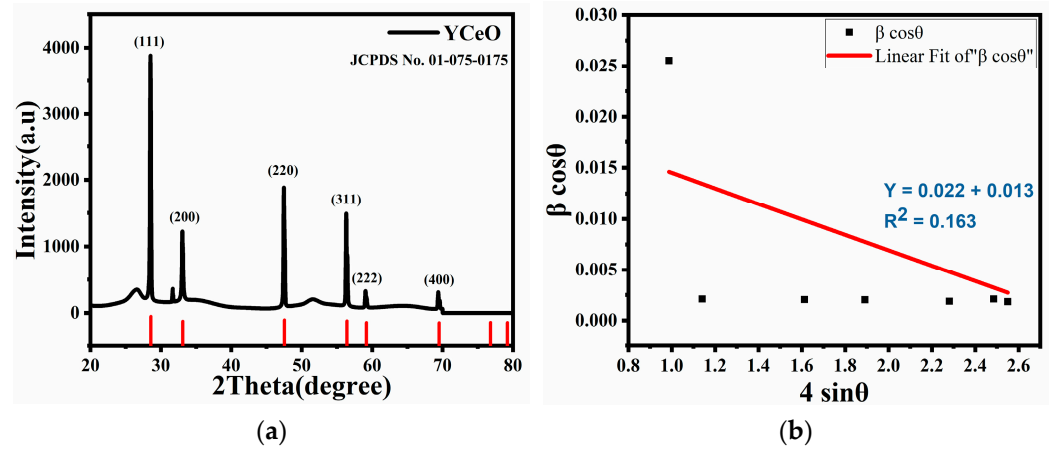


Figure 1. (a) XRD pattern of YCeO and (b) shows the graph of W.H plot.

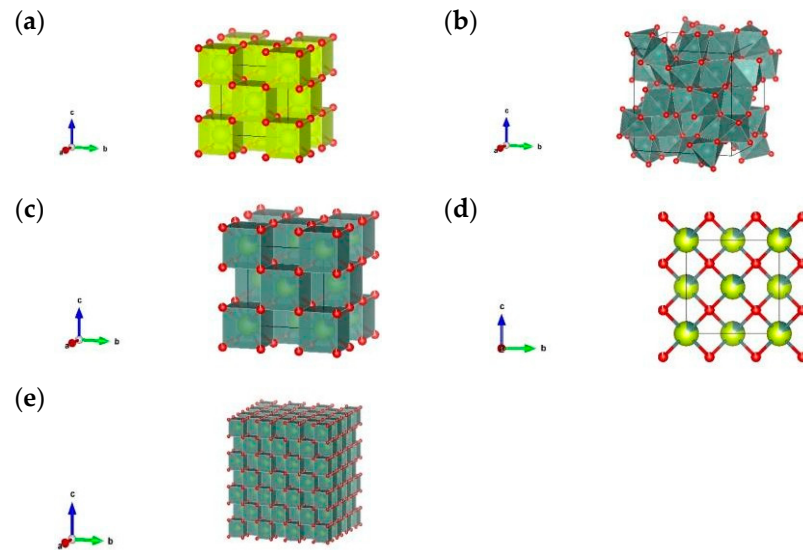


Figure 2. Different crystals of YCeO. (a) the structure of CeO₂, (b) the structure of Y₂O₃, (c) the complete crystal structure of cubic YCeO, (d) the single layer of YCeO, (e) multilayer crystal cubic structure of YCeO.

Table 1. Calculated structural parameters of YCeO crystal structure.

S. No	Calculated Parameters	YCeO
1.	Empirical Formula	Ce _{0.80} O _{1.90} Y _{0.20}
2.	Chemical Formula	Y _{0.20} Ce _{0.80} O _{1.90}
3.	Lattice system	Cubic
4.	Crystal system	Cubic
5.	Space group	Fm3m
6.	Space number	225
7.	a (Å)	5.4040
8.	b (Å)	5.4040
9.	c (Å)	5.4040
10.	α (°)	90
11.	β (°)	90
12.	γ (°)	90
13.	Density (gm cm ⁻³)	6.74

Table 1. *Cont.*

S. No	Calculated Parameters	YCeO
14.	Volume (10^6) pm^3	157.81
15.	Z (no. of molecules)	4
16.	RIR (Reference intensity ratio)	13.60
17.	Crystallite (grain) size (nm)	18.66
18.	Lattice Strain	0.0041
19.	Dimensionality	3D
20.	Degree of Freedom	6
21.	R-Square (COD)	0.16363
22.	Adj. R-Square	0.02423

The Williamson–Hall plot ($\beta \cos\theta$ vs. $\sin\theta$) is attained from XRD results. As the laser effect increases, the slope of the Williamson–Hall plot increases. Due to strain toughening, the size of the diffraction peak increases as a result of the increase in lattice strain and the decrease in crystallite size. Crystal imperfections and distortion of strain-induced peak broadening are related by $\varepsilon \approx \beta s / \tan\theta$. Scherrer-equation follows a $1/\cos\theta$ dependence but not $\tan\theta$ as the W–H method. Dependent on dissimilar θ positions, the parting of size and strain broadening examination is conducted using Williamson and Hall, the graph shown in Figure 1.

3.2. FE-SEM Analysis

In examining the interactions between nanomaterials, the purity and shape of the nanoparticles are unquestionably essential elements. The two nanoparticles are therefore measured using a FESEM and the results are presented. Both nanoparticles generally showed the same morphology as fused and aggregated nanoparticles. Field emission scanning electron microscopy was performed for a better understanding of the structure and morphology; Figure 3 shows the image taken from FE-SEM at 100 nm and shows the surface morphology and calculated average particle size of 206.68 nm in the particle.

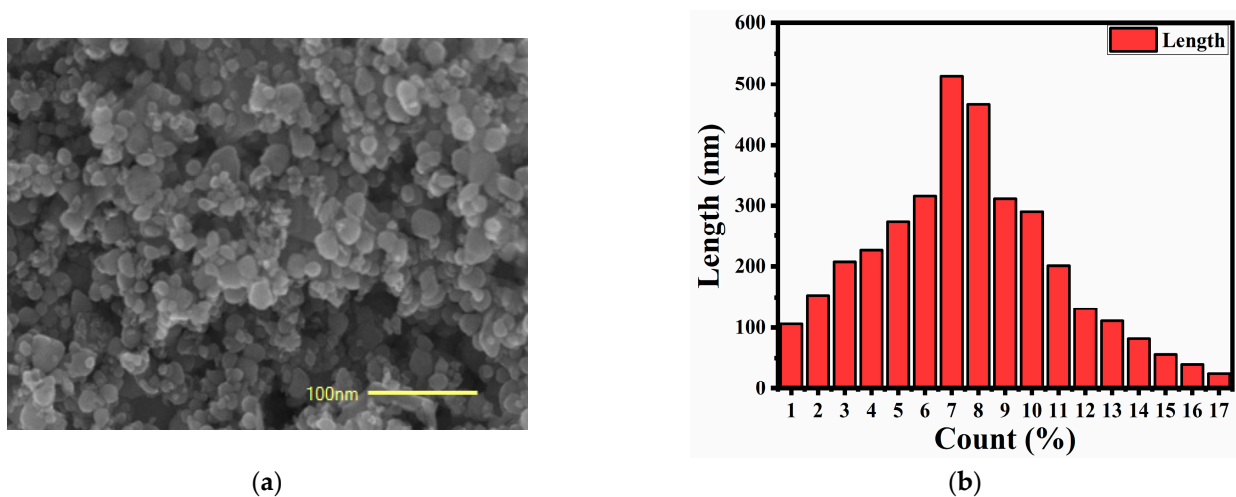


Figure 3. (a) shows the FE-SEM micrograph of YCeO under 100 nm and (b) shows the average particle distribution size which was calculated by the micrograph image FE-SEM.

3.3. AFM Analysis

For quantitatively determining the nanometric dimensional surface roughness and for seeing the surface nano-texture of the deposited film, atomic force microscopy examination is the best option. The surface of the as-grown YCeO films has a granular texture, as seen in the AFM images in Figure 4, which is comparable to that seen in the SEM investigations. The crystallites are larger in the AFM images, though, because of tip convolution. The SEM

photos show that the borders of the tiny spaces between the grains appear to be less crisp for the same reason. In contrast to the “hill” region, which is made up of numerous crystal-like structures that have certain orientations, the “valley” region is comparatively smooth. As calculated, its RMS (root mean square) roughness was 50.82 nm, mean roughness was 40.49, and average became 126.1 nm.

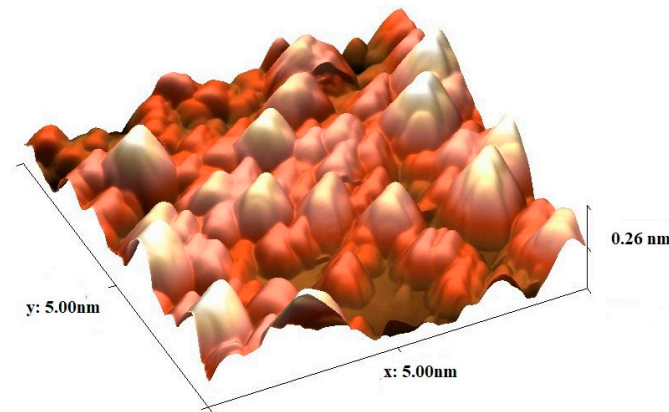


Figure 4. The 3D view of the AFM micrograph observed of a yttrium cerium oxide nanoparticle in the nanometer range.

3.4. Nanoparticle Size Analyzer

The size of each particle as well as the size distribution range for a certain sample is determined using a nanoparticle size analyzer. In the study of nanoparticle characteristics and the interaction of cell materials, size distribution is a crucial and highly favorable feature. The size of the YCeO particles in deionized water is shown in Figure 5. According to the DLS measurement, the YCeO’s average particle size was 690 nm in 100%. Those have a particle distribution peak from 359.09 to 1726.40 nm. The increased particle size (found through DLS measurement) may be due to anticipated agglomerations and dynamic scattering of the nanoparticles in the dispersion medium [18].

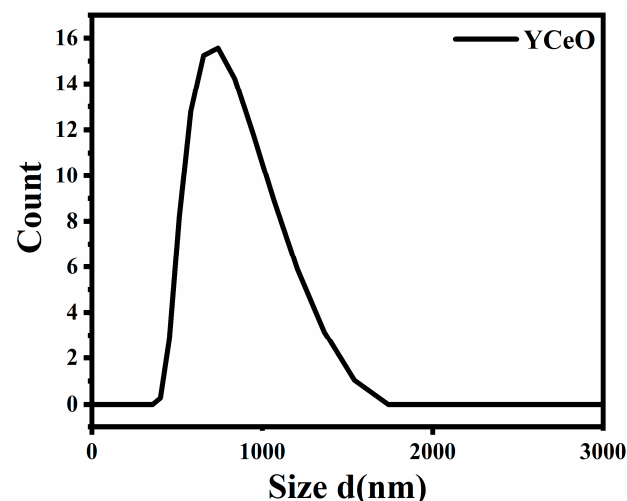


Figure 5. Graph of nanoparticle size distribution.

3.5. FTIR Spectroscopy Analysis

To determine the chemical integrity of the tested nanoparticles, FTIR measurements were carried out. The spectra are shown in Figure 6 with wave numbers ranging from 400 to 4000 cm^{-1} . The O-H stretching vibration in OH groups is the cause of the large bandwidth that is specifically seen at 3000–3500 cm^{-1} , according to the details of the observation.

The bands observed between 1250 and 1750 cm^{-1} are caused by the asymmetric stretching of the C-O band, which may result from the absorption of CO_2 from the environment. The bands seen at about 750 cm^{-1} are attributed to the Y-O bond stretching vibration as closed, with the wave number stated in the earlier investigation by Schwartz and Schwartz [19]. It can be shown from the FTIR analysis that the sample is a mixed composite of cerium and yttrium oxide. The lattice vibration modes of M-O and O-M-O correspond to the bands in the low-frequency range of 400 cm^{-1} to 1000 cm^{-1} (Ce, Y). The fact that the YO absorption bands are wider in Ce1/Y2 samples than they are in Ce2/Y1 samples suggests this [3].

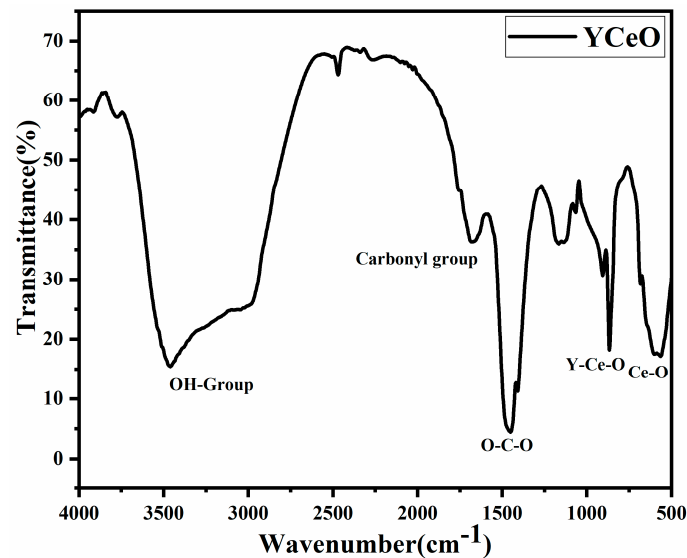


Figure 6. FTIR spectra of yttrium cerium oxide nanocomposite.

3.6. UV-Visible Spectroscopy Analysis

Figure 7 illustrates the YCeO UV-vis (250–900 nm) absorption spectrum. Around 256.58 nm in the UV area is where the absorption was discovered. Particle size distribution and flaws may be to blame for the gradual increase in absorbance and broadening of the absorbance peak [19]. According to Equations (3) and (4) of Beer's relation, Lambert's absorption coefficient (α) can be calculated: where x is the cuvette's thickness, I_0 is the initial photon intensity, and I is the instantaneous photon intensity,

$$I = I_0 e^{-\alpha x} \quad (3)$$

$$\alpha(\lambda) = [\ln(I_0/I)]/x = [\ln T/x] = 2.303A/x \quad (4)$$

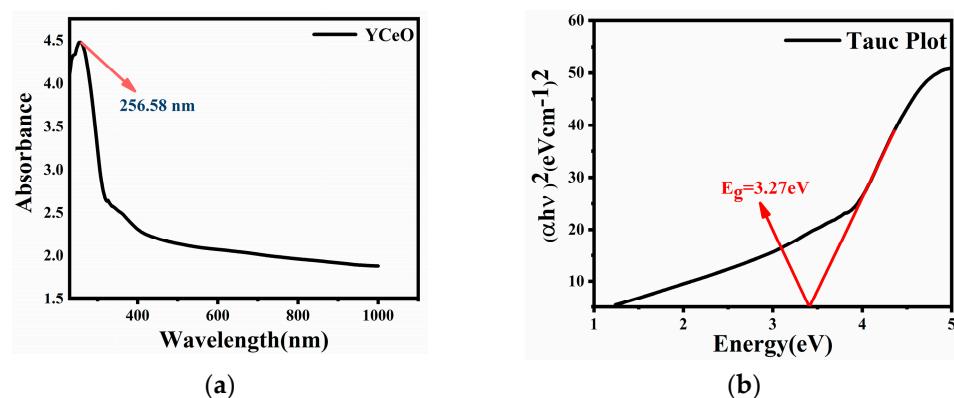


Figure 7. (a) shows the UV-visible absorption spectra and (b) shows the band gap of yttrium cerium oxide nanocomposite.

The transition between extended states in the valence and conduction bands is what causes the greater value of the structure in the UV region (330–400 nm). Using Tauc's figure, the value of the optical energy band gap for YCeO was examined. To calculate the optical band gap, Tauc's relation from Equation (5) was employed (Eg) [20].

$$\alpha = [\alpha_0 (h\nu - E_g)^n]/h\nu \quad (5)$$

Here, the photon energy ($h\nu$), the absorbance coefficient (α), the characteristic parameter (α_0), Planck's constant (h), and the power factor (n) are all defined. Depending on the nature of the transition, n may take on different values. Since the transition, in this case, is of the directly authorized kind, the value of n is taken to be $\frac{1}{2}$ what Eg for YCeO is calculated to be 3.27 eV.

3.7. TGA Analysis

To quantify the thickness of the coating on the nanoparticle's surface, thermogravimetric analysis (TGA) might be utilized. This estimate offers details on both chemical and physical events, including stage shifts, ingestion, adsorption, desorption, composition, purity, decomposition reactions, decomposition temperatures, and absorbed moisture content. Thermal analysis, in its broadest sense, refers to a method for determining the temperature and time at which a substance undergoes physical changes when heated or cooled. TGA is a crucial tool for viewing particles at various temperatures since an object's temperature affects the mobility of its particles (the higher the temperature, the faster the particles must move to maintain stability). From Figure 8 where 0.83% of the weight is lost at 200 °C and at last only 1.15% of the weight is lost up to 1000 °C, it can be shown that yttrium cerium oxide nanocomposite has better stability at high temperatures also.

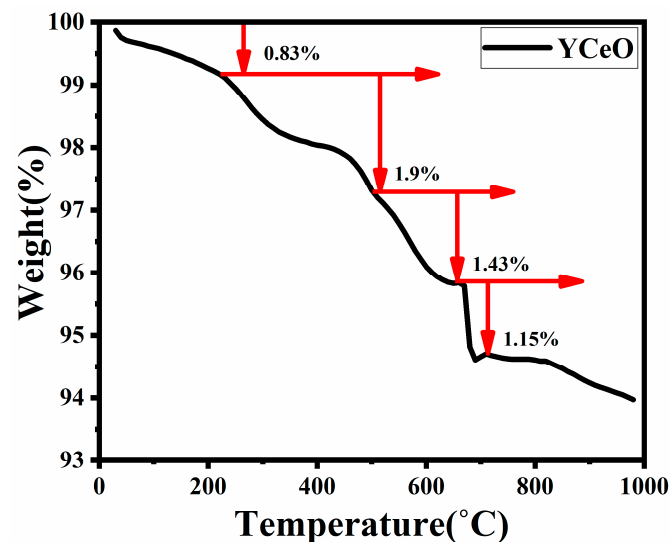


Figure 8. The TGA graph observed of yttrium cerium oxide nanoparticles for thermal stability.

3.8. BET Analysis

Using the Brunauer–Emmett–Teller (BET) analytical physical characterization approach, solid materials' precise surface areas and porosity distributions are quantified. A wide variety of solid matrices, including monolithic materials and catalyst powders, can be used using this approach [21]. In this present work BET with nitrogen dioxide at a saturated pressure of 101.54 [kPa], a sample weight of 0.05 g with 9.792 slandered volume at an adsorption temperature of 77 k was used. We observed the volume of YCeO was 1.8573 cm³/g, and the specific surface area was calculated as 8.084 m²/g which is shown in Figure 9, where the pore graph of the material shows its porosity, from this, the relative pressure or total pore volume (p/p_0) was 0.090 cm³/g, and the mean pore diameter calculated was 44.983 nm. Hence, it was observed that YCeO has a great specific surface

area and porous material which proves that this material has to play a great and prominent role in many applications.

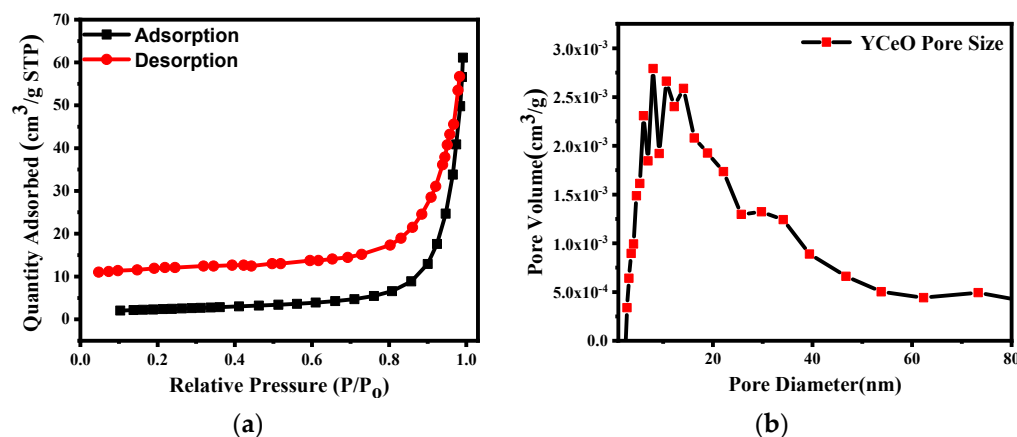


Figure 9. (a) shows the adsorption and desorption of NO₂ and (b) shows the pore size of YCeO.

4. Conclusions

In this present work, the rare earth metal yttrium cerium oxide was synthesized through one-step hydrothermal synthesis using yttrium nitrate (III) hexahydrate and cerium nitrate (III) hexahydrate as starting precursors. XRD characterization was performed for understanding the structure of YCeO nanocomposite and found a well-shaped cubic structure and many more parameters calculated from Xpert Highscore and Fullprof software. For a complete analysis of the structural morphology, FE-SEM was performed, and the calculated average particle size was 206.68 nm. Further, AFM was performed for the surface roughness, and DLS measurement was performed to obtain an average particle size peak and the distribution was 690 nm and 359.09 to 1726.40 nm. FTIR confirmed the functional groups present, UV-visible observed the wavelength of 256.68 nm and found the band gap of 3.27 eV, TGA confirmed the nanocomposite stability up to 1000 °C, and lastly, BET found the specific surface area of YCeO was 8.084 m²/g and the mean pore diameter was 44.983 nm. This report purely focused on the structural and morphological properties of yttrium cerium oxide nanocomposite and found that yttrium cerium oxide contains a high specific surface area and has an average particle size which plays an important role in the adsorption process, heterogeneous catalysis, detection of molecules in a gaseous environment, biological applications, and many more. This YCeO nanocomposite synthesized using a low-cost technique is suitable for a wide range of applications such as sensors, industry, automobiles, etc.

Supplementary Materials: The following supporting information can be downloaded at: <https://www.mdpi.com/article/10.3390/IOCN2023-14542/s1>, Presentation Video: Low-Cost Hydrothermally Synthesized Multifunctional Rare Earth Metal Yttrium Cerium Oxide.

Author Contributions: Visualization, writing, graphics, and characterization: S.S.; supervision, formal analysis, visualization: N.K.P. All authors have read and agreed to the published version of the manuscript.

Funding: This research received no external funding.

Institutional Review Board Statement: Not applicable.

Informed Consent Statement: Not applicable.

Data Availability Statement: Data will be available on demand.

Acknowledgments: The authors would like to thank my supervisor or guide as well as our Head of Department, N.K. Pandey (University of Lucknow) for always supporting us. Secondly, I would like to thank Mohammad Abu Sazz (Banaras Hindu University) for helping me with the research synthesis.

Third, I would like to thank Rajiv Prakash, Dean (IIT BHU) for helping me to use the hydrothermal technique. I would also thank to the CIF (Central instrument facility) of IIT BHU for helping in the XRD, TGA, and BHU for using AFM. Thanks to BSIP Lucknow for the FE-SEM characterization, and lastly the chemistry department at University of Lucknow for use of the UV-visible and FTIR facility and chemistry department, BBAU for BET facility.

Conflicts of Interest: The authors declare no conflict of interest.

References

1. Zhang, C.; Zhang, X.; Wang, Y.; Xie, S.; Liu, Y.; Lu, X.; Tong, Y. Facile electrochemical synthesis of CeO₂ hierarchical nanorods and nanowire with excellent photocatalytic activities. *New J. Chem.* **2014**, *38*, 2581–2586. [[CrossRef](#)]
2. Goharshadi, E.K.; Samiee, S.; Nancarrow, P. Fabrication of cerium oxide nanoparticles: Characterization and optical properties. *J. Colloid Interface Sci.* **2011**, *356*, 473–480. [[CrossRef](#)] [[PubMed](#)]
3. Kaviyarasu, K.; Manikandan, E.; Nuru, Z.Y.; Maaza, M. Investigation on the structural properties of CeO₂ nanofibers via CTAB surfactant. *Mater. Lett.* **2015**, *160*, 61–63. [[CrossRef](#)]
4. Ameta, K.L.; Papnai, N.; Ameta, R. Photocatalytic Degradation of Malachite Green Using Nano-sized cerium-iron Oxide. *Orbital Electron. J. Chem.* **2014**, *6*, 4–19.
5. Magdalene, C.M.; Kaviyarasu, K.; Vijaya, J.J.; Jayakumar, C.; Maaza, M.; Jeyaraj, B. Photocatalytic degradation effect of malachite green and catalytic hydrogenation by UV-illuminated CeO₂/CdO multilayered nanoplatelet arrays: Investigation of antifungal and antimicrobial activities. *J. Photochem. Photobiol. B Biol.* **2017**, *169*, 110–123. [[CrossRef](#)]
6. Gu, S.; Chen, Y.; Yuan, X.; Wang, H.; Chen, X.; Liu, Y.; Jiang, Q.; Wu, Z.; Zeng, G. Facile synthesis of CeO₂ nanoparticles sensitized CdS nanorods photocatalyst with improved visible-light photocatalytic degradation of Rhodamine B. *RSC Adv.* **2015**, *5*, 79556–79564. [[CrossRef](#)]
7. Askarnejad, A.; Morsali, A. Syntheses and characterization of CdCO₃ and CdO nanoparticles by using a sonochemical method. *Mater. Lett.* **2008**, *62*, 478–482. [[CrossRef](#)]
8. Zhao, M.; Li, H.; Shen, X.P.; Ji, Z.Y.; Xu, K.Q. Facile electrochemical synthesis of CeO₂@Ag@CdS nanotube arrays with enhanced photoelectrochemically water splitting performance. *Dalton Trans.* **2015**, *44*, 19935–19941. [[CrossRef](#)]
9. Couture, P.; Williams, G.V.M.; Kennedy, J.; Leveneur, J.; Murmu, P.P.; Chong, S.V.; Rubanov, S. Multiferroic nanocrystalline BiFeO₃ and BiCrO₃ thin films prepared by ion beam sputtering. *Int. J. Nanotechnol.* **2017**, *14*, 56–65. [[CrossRef](#)]
10. Couture, P.; Williams, G.V.M.; Kennedy, J.; Leveneur, J.; Murmu, P.P.; Chong, S.V.; Rubanov, S. Nanocrystalline multiferroic BiFeO₃ thin films made by room temperature sputtering and thermal annealing, and formation of an iron oxide-induced exchange bias. *J. Alloys Compd.* **2017**, *695*, 3061–3068. [[CrossRef](#)]
11. Kennedy, J.; Fang, F.; Futter, J.; Leveneur, J.; Murmu, P.P.; Panin, G.N.; Kang, T.W.; Manikandan, E. Synthesis and enhanced field emission of zinc oxide incorporated carbon nanotubes. *Diam. Relat. Mater.* **2017**, *71*, 79–84. [[CrossRef](#)]
12. Porqueras, I.; Pearson, C.; Corbella, C.; Vives, M.; Pinyol, A.; Bertran, E. Characteristics of e-beam deposited electrochromic CeO₂ thin films. *Solid State Ion.* **2003**, *165*, 131–137. [[CrossRef](#)]
13. Zhao, S.; Li, J.; Wang, L.; Wang, X. Degradation of Rhodamine B and Safranin-T by MoO₃:CeO₂ Nanofibers and Air Using a Continuous Mode. *Clean-Soil Air Water* **2010**, *38*, 268–274. [[CrossRef](#)]
14. Frazer, K.A.; Pachter, L.; Poliakov, A.; Rubin, E.M.; Dubchak, I. VISTA: Computational tools for comparative genomics. *Nucleic Acids Res.* **2004**, *32*, W273–W279. [[CrossRef](#)]
15. Baldinozzi, G.; Berar, J.-F.; Calvarin, G. Rietveld refinement of two-phase Zr-doped Y₂O₃. *Mater. Sci. Forum* **1998**, *278-281*, 680–685. [[CrossRef](#)]
16. Artini, C.; Costa, G.A.; Pani, M.; Lausi, A.; Plaisier, J. Structural characterization of the CeO₂/Gd₂O₃ mixed system by synchrotron X-ray diffraction. *J. Solid State Chem.* **2012**, *190*, 24–28. [[CrossRef](#)]
17. Brauer, G.; Gradinger, H. Über heterotype Mischphasen bei Seltenerdoxyden. I. *J. Inorg. Gen. Chem.* **1954**, *276*, 209–226.
18. Mahapatra, C.; Singh, R.K.; Lee, J.H.; Jung, J.; Hyun, J.K.; Kim, H.W. Nano shape varied cerium oxide nanomaterials rescue human dental stem cells from oxidative insult through intracellular or extracellular actions. *Acta Biomater.* **2017**, *50*, 142–153. [[CrossRef](#)]
19. Traina, C.A.; Schwartz, J. Surface modification of Y₂O₃ nanoparticles. *Langmuir* **2007**, *23*, 9158–9916. [[CrossRef](#)] [[PubMed](#)]
20. Verma, A.; Chaudhary, P.; Tripathi, R.K.; Yadav, B.C. Transient photodetection studies on 2D ZnO nanostructures prepared by simple organic-solvent assisted route. *Sens. Actuators A Phy.* **2021**, *321*, 112600. [[CrossRef](#)]
21. Hassellöv, M.; Readman, J.W.; Ranville, J.F.; Tiede, K. Nanoparticle analysis and characterization methodologies in environmental risk assessment of engineered nanoparticles. *Ecotoxicology* **2008**, *17*, 344–361. [[CrossRef](#)] [[PubMed](#)]

Disclaimer/Publisher's Note: The statements, opinions and data contained in all publications are solely those of the individual author(s) and contributor(s) and not of MDPI and/or the editor(s). MDPI and/or the editor(s) disclaim responsibility for any injury to people or property resulting from any ideas, methods, instructions or products referred to in the content.